scientific reports

Check for updates

OPEN

A study of rare earth elements enriched carbonisation material prepared from *Dicranopteris pedata* biomass grown in mining area

Liujun Feng[1], Zhiqiang Chen[1]✉, Haiyan Wang[1], Zhibiao Chen[1], Zuliang Chen[2]✉, Jianhua Liu[1] & Yuee Zeng[3]

Phytoremediation is currently a very popular remediation method for salvaging rare earth mining sites. However, there is still a challenge concerning how to use secondary resources such as plant biomass following the extraction of rare earth elements (REEs). Herein, *Dicranopteris pedata* (Houtt.) Nakaike, a REEs hyperaccumulator, served to fabricate REEs-rich carbonisation materials (REEs/C) at different temperatures. The results showed that the percentages of Pb(II) removed using REEs/C prepared at 400 °C (REEs/C-4) and 800 °C (REEs/C-8) were 85.1% and 84.0%, respectively. These amounts were better than that of REEs-C prepared at 600 °C (REEs/C-6 (67.0%)). Characterisation analysis confirmed that rich functional groups like aromatic, hydroxyl and C = C/C-C in REEs/C-4 provided more chelation sites to effectively complex with Pb(II), while the superior removal capacity of REEs/C-8 resulted from the enrichment of more REEs and abundant pore structure. Chemisorption, such as ion exchange and chelation, plays a significant role in adsorption. During the carbonisation process of REEs/C, the REEs enriched in *Dicranopteris pedata* contributed to the formation of rare earth oxides and oxygen vacancies in the material, and these properties enhanced the Pb removal ability of REEs/C. Moreover, the REEs contained in the material did not cause a leaching phenomenon during Pb removal, which is a safe and environmentally friendly material. Finally, the REEs/C was applied to wastewater, and it was found that this material could effectively adsorb Pb from wastewater. Overall, this study generates a new insight into: firstly, how to use phytoextracted biomass containing REEs as valuable REEs/C materials; and secondly, how to save the environment by using technology that promotes recycling of used materials.

Keywords *Dicranopteris pedata*, Rare earth elements/Carbonisation material, Pb(II), Chemisorption, Oxygen functional groups, Wastewater

The mining and consumption of rare earth elements (REEs) in China is the largest in the world, and the ionic-adsorption-type Rare Earth Mine areas (IREMs) in southern China are rich in REEs, which are widely used in various fields. However, major mining techniques, whether "pond leaching" and "heap leaching" in the past or in situ leaching as currently utilised, all discard surface plants and topsoil in the mining area, triggering very serious environmental damage, such as desertification, soil erosion, biodiversity loss, heavy metals toxicity/pollution, and groundwater pollution. In particular, heavy metal and groundwater pollution too often spread to adjacent farmlands and villages, putting human health at great risk[1]. Research has found that REEs - due to their toxic and carcinogenic characteristics - can accumulate in the liver and other reticular structures of the body, leading to hepatotoxic and neurotoxic outcomes and lung damage[2]. Thus, the environmental deterioration that is evident in IREM has become a key issue in the rare earth mining industry and garnered the attention of scientists in recent decades.

At present, ecological restoration technologies in mine areas usually include physical, chemical, and biological treatment strategies. Phytoremediation, a type of bioremediation technology, is a rehabilitation method utilising plants to restore vegetation, reduce soil and water loss, remove hazardous pollutants in ore districts,

[1]School of Geographical Science, Fujian Normal University, Fuzhou 350117, Fujian Province, China. [2]College of Environmental and Resource Science, Fujian Normal University, Fuzhou 350117, Fujian Province, China. [3]School of Resources and Environmental Sciences, Quanzhou Normal University, Quanzhou 362000, Fujian Province, China. ✉email: soiltuqiang061@163.com; zlchen@fjnu.edu.cn

and ultimately improve or save the local environment[3]. The key to phytoremediation is selecting appropriate hyperaccumulators, and species that grow locally in IREM are generally the best choice. In comparison with traditional techniques, phytoremediation has some unique advantages such as cost-effectiveness, energy-efficiency, and environmental friendliness. Our previous field work discovered that the dominant vegetation species in IREM are *Dicranopteris pedata* (Houtt.) Nakaike and *Pinus massoniana* Lamb., the results confirm that *Dicranopteris pedata* can grow on acidic (pH 4–5), poor and dry soil due to its high nutrient- and water-use efficiency[4,5]. In fact, *Dicranopteris pedata* is a clonal plant which can asexually reproduce through underground stems. Subsequently, it demonstrates high survivability so that it can always form dominant communities at IREM in south China, and always form pure formations[4].

Dicranopteris pedata and *Phytolacca americana* L. are typical rare-earth hyperaccumulators that have long received attention and studies by researchers[6,7]. Among them, *Dicranopteris pedata* is a dominant species in rare-earth mining areas. Our previous work discovered that the concentration of REEs in *Dicranopteris pedata* can be as high as 2364.51 $mg{\cdot}kg^{-1}$, while the content in other species only ranged from 6.81 to 92.17 $mg{\cdot}kg^{-1}$ in IREM in Changting County, China[8]. The distribution pattern of REEs in *Dicranopteris pedata* has been revealed. For example, Wei et al.[6] found that the REEs of different subcellular fractions of *Dicranopteris pedata* leaves were cell wall > organelles > 'soluble' fraction (i.e. cytoplasmic solutes and vesicles) > cell membrane. It has also been reported that silica pectin matrix fixation is a key mechanism for detoxification in rare earth hyperaccumulator[9]. Therefore, *Dicranopteris pedata* can be used for soil remediation in rare earth mining areas. After extracting rare earths, clipping has become an essential part of *Dicranopteris pedata* remediation of mine soils. Related studies have paid attention to the clipping after phytoremediation[10]. *Dicranopteris pedata* proved to be effective in controlling the migration of REEs when the coverage threshold reached 70%[11]. Additionally, *Dicranopteris pedata* has significant functions to play in ecosystem soil and water conservation and landscape restoration[5]. Based on these findings, we proposed a new strategy using *Dicranopteris pedata* clipping to remediate the environment around IREMs, and revealed excellent restorative effects in 4 IREMs in Changting County, Fujian Province, China[12]. However, improper disposal of waste after clipping *Dicranopteris pedata* caused secondary pollution to the environment, which means that the technology requires more refinement if it is to work properly. Based on environmental concerns with cleaner and more sustainable solutions, how to treat hyperaccumulator biomass after extracting soil REEs is a critical issue.

It is reported that the doping of REEs into magnetic carbonisation material can significantly enhance the adsorption of phosphate, indicating the potential value of REEs[13]. Nevertheless, such additional REEs doping is unstable, which may affect the reactivity of the composite[13,14]. To address these questions, we proposed that *Dicranopteris pedata* be a precursor to one-step fabrication of REEs-enriched carbonisation materials (REEs/C) at different carbonisation temperatures. Here, the key gaps in our knowledge to be resolved require answers to the following questions: (1) what are the differences in the chemical composition and surface properties at different calcination temperatures; and (2) can the REEs/C be deployed to remove heavy metals such as Pb(II).

To solve the above issue, we collected a sample of *Dicranopteris pedata* from the rare earth mining area and turned it into REEs/C under three temperatures for the purposes of characterisation. The performance of carbonisation materials was also tested by experiments conducted to remove Pb(II). Our analysis could solve a key issue of *Dicranopteris pedata* functioning as a restoration technology: how to dispose of and recycle the *Dicranopteris pedata* clipping waste biomass. This work provides a new theoretical understanding of and technical methods for soil and water conservation and ecological restoration in southern China's rare earth mining areas, which can help the rare earth mining industry be environmentally responsible.

Materials and methods

Chemical reagents and raw materials

Lead nitrate ($Pb(NO_3)_2$) was purchased from Aladdin Reagent (Shanghai) Co. Ltd., and was of analytical grade. Waste samples of *Dicranopteris pedata* were sourced from the rare earth ore region in Hetian Town, Changting County, Fujian Province, China (116°26′11″E, 25°40′29″N). The concentrations of *Dicranopteris pedata* and soil from that mine are indicated in Table 1.

REEs ($mg{\cdot}kg^{-1}$)	Soil	Dicranopteris pedata	REEs ($mg{\cdot}kg^{-1}$)	Soil	Dicranopteris pedata
La	233.97	1059.00	Dy	35.03	11.62
Ce	104.43	916.30	Ho	6.66	1.78
Pr	52.96	226.70	Er	19.66	6.12
Nd	195.02	934.20	Tm	2.74	0.50
Pm	Undetectable by ICP-MS		Yb	18.51	2.67
Sm	40.60	86.70	Lu	2.55	0.35
Eu	7.39	9.52	Sc	11.28	11.54
Gd	42.29	63.52	Y	190.07	45.56
Tb	6.21	4.29	∑REEs	969.35	3420.37

Table 1. REEs concentrations of *Dicranopteris pedata* and soil from a rare earth ore region ($n = 5$).

Preparation of REEs/C

Firstly, we dried the *Dicranopteris pedata* sample of waste for 72 h at 65 °C and ground it to a fine powder so that it could pass through a 100-mesh sieve. The *Dicranopteris pedata* powder was then dried for 3 h at 65°C. Secondly, appropriate amounts of powder of *Dicranopteris pedata* were calcined in a tube furnace at 400°C, 600°C, and 800°C separately under a nitrogen atmosphere for 3 h, the heating rate being 5°C min^{-1}. Thirdly and finally, the REEs/C was cooled to room temperature and stored in a zip-lock bag in a dryer. The REEs/C samples derived from *Dicranopteris pedata* clipping waste at 400°C, 600°C, and 800°C were named., respectively, REEs/C-4, REEs/C-6, and REEs/C-8.

Characterization experiments

A Thermogravimetric Analyzer (TGA, Q500, TA, USA) measured the mass variation of REEs/C prepared by *Dicranopteris pedata* clipping at a heating rate of 5 °C min^{-1} to a final temperature of 1000 °C. The functional groups present in *Dicranopteris pedata* REEs/C with 3 calcination temperatures were monitored by Fourier Infrared Spectrometer (FTIR, NICOLET IS10, Thermo Fisher Scientific, USA) in the wavelength range of 4000 –400 cm^{-1}. Crystal structure discrepancies in *Dicranopteris pedata* REEs/C with different preparation temperatures were determined using X-ray Powder Diffractometer (XRD, D8 ADVANCE, Bruker, Germany) at 2θ of 5° – 75° and increment of 0.02 s^{-1}. The specific surface areas of *Dicranopteris pedata* REEs/C with different preparation temperatures were obtained from Brunauer-Emmett-Teller (BET, BELSORP-mini II, Japan), based on N_2 adsorption and desorption curves.

The morphological and elemental compositions of *Dicranopteris pedata* REEs/C with different preparation temperatures were detected by Ultrahigh resolution cold field emission scanning electron microscope (SEM, Regulus 8100, Hitachi, JPN). It was combined with EDS (JEM-2100, Lorentz) using an acceleration voltage of 5.2 kV. Differences on the surface elemental composition and speciation of *Dicranopteris pedata* REEs/C with different preparation temperatures were analysed by Multifunctional imaging electron spectrometer (XPS, Thermo ESCALAB 250XI, Thermo Fisher Scientific, USA). Here the test parameters were ALKα (hv = 1486.6 eV), 150 W, 500 μm, and the calibration point of the binding energy of the instrument was C1s = 284.8 eV. The electrical charge characteristics of REEs/C with different preparation temperatures were measured using a Zeta point position analyser in different pH (NANO ZS, Malvern Panalytical, UK).

Removal experiment

To evaluate the removal capacity of various REEs/C, we designed an experiment for removing Pb(II) utilising three tested REEs/Cs. Briefly, REEs/C (0.05 g) and 15 $mg{\cdot}L^{-1}$ $Pb(NO_3)_2$ solution (50 ml) were put into a 150 ml transparent glass conical flask together. Then, it was shaken at 30°C and 250 rpm for 90 min to ensure sufficient reaction between REEs/Cs and lead nitrate solution. Ultimately, a pure $Pb(NO_3)_2$ solution was obtained by filtration through a 0.22 μm filter for analysis using Atomic Absorption Spectrometer (AAS, VARIAN AA240, USA). The concentration of REEs in solution was analysed by Inductively Coupled Plasma Mass Spectrometry (ICP-MS, X-Series 2, Thermo Scientific, Massachusetts, USA). Three replicates were set up for all treatments.

The removal experiment of heavy metal in mine wastewater was designed to test the potential of REEs/C for practical applications. Briefly, REEs/C (0.1 g) was placed in a 150 ml clear glass conical flask along with actual wastewater (50 ml) from a mine in Fujian Province. Then, it was shaken at 30 °C and 250 rpm to ensure sufficient reaction between REEs/Cs and lead nitrate solution. Finally, 1 mL was sampled at 0.5, 1, 4, 8, 12, 24, 48, and 72 h. The solution to be measured was obtained by filtration through a 0.22 μm filter, and was used to detect the concentration of each heavy metal ion using ICP-MS. Three replicates were set up for all treatments.

Adsorption model

Pseudo-first-order, pseudo-second-order, Elovich and intraparticle diffusion models (Eqs. 1–4) were used to explore the kinetic parameters and adsorption mechanisms[15].

$$Q_t = Q_e(1 - e^{-K_1 t}) \tag{1}$$

$$Q_t = \frac{K_2 Q_e^2 t}{1 + K_2 Q_e t} \tag{2}$$

$$Q_t = \frac{1}{\beta}\ln(\alpha\,\beta\,t + 1) \tag{3}$$

$$Q_t = K_{int} t^{1/2} + C \tag{4}$$

where Q_t (mg g^{-1}) and Q_e (mg g^{-1}) are the adsorbed amounts of HMs at time t and at adsorption equilibrium, respectively; K_1 (min^{-1}), K_2 (g (mg min)$^{-1}$), and K_{int} (mg g^{-1} s^{-1}) are pseudo-first-order and pseudo-second-order adsorption kinetic model and intraparticle diffusion model constants, respectively; α (mg g^{-1} s^{-1}) and β (g mg^{-1}) are the Elovich adsorption kinetic model rate constants for adsorption and desorption at time t, and C (mg g^{-1}) is a constant.

Meanwhile, Langmuir and Freundlich (Eqs. 5 and 6) adsorption isotherm model was used to explore the adsorption mechanism[16].

$$Q_e = \frac{q_{max} K_L C_e}{1 + K_L C_e} \tag{5}$$

$$R_L = \frac{1}{1 + K_L C_0} \tag{6}$$

Where q_{max} (mg g^{-1}) represents the maximum adsorption amount, Q_e (mg g^{-1}) is the equilibrium adsorption amount, C_0 (mg g^{-1}) is the initial concentration of HMs in the solution and C_e (mg g^{-1}) is the concentration of HMs in the solution at equilibrium; K_L (L mg^{-1}) and K_F (mg^{1-n} L^n g^{-1}) are the Langmuir and Freundlich models respectively adsorption constants; n is the exponent of the Freundlich model.

The thermodynamic parameters enthalpy of adsorption (ΔH°), entropy of adsorption (ΔS°) and Gibbs free energy (ΔG°) were determined by the Eyring equation (Eqs. 7–9)[17]:

$$K_d = \frac{Q_e}{C_e} \tag{7}$$

$$\Delta G^{\circ} = -RT\ln(K_d) \tag{8}$$

$$\ln(K_d) = \frac{T\Delta S^{\circ} - \Delta H^{\circ}}{RT} \tag{9}$$

Where Kd (L g^{-1}) is the distribution coefficient, r (J mol^{-1} K^{-1}) and T (K) are the ideal gas constant and the absolute temperature of the aqueous solution, respectively. ΔH° and ΔS° are determined from the slope and intercept of the linear plot of ln(Kd).

Statistical analysis

The experiment data was collected and organised using MS Excel 2019 (Microsoft Corp., Redmond, WA, USA). IBM SPSS Statistics 22.0 (IBM Corp., Armonk, NY, USA) was used for statistical analysis of the data. Shapiro-Wilk test was used to test whether the data conformed to a normal distribution, and a homogeneity of variance test was done on the data. After passing the test, one-way analysis of variance (ANOVA) was used to compare the differences between treatments. The differences in group means were tested using the least-significant difference test with a significance level of $P < 0.05$. All illustrations were generated using Origin Pro 2022 (Origin Lab Corp., Northampton, MA, USA).

Results and discussion

Removal performance of three tested REEs/C

The performance of three REEs/C for the removal of Pb(II) is shown in Fig. 1a. After being exposed to REEs/C-4 and REEs/C-8 for 90 min, the efficiency in removing Pb(II) reached 85.09% and 83.96%, respectively. ANOVA test analysis showed no significant difference between the removal rates of REEs/C-4 and REEs/C-8 ($P > 0.05$). However, only 66.95% of Pb(II) was removed by REEs/C-6, which was remarkably less than REEs/C-4 and REEs/C-8 ($P < 0.05$). Pb(II) removal experiments confirmed that the use of REEs/C prepared from *Dicranopteris pedata* clipping waste has great potential as pollutant-removing materials. Furthermore, it was observed that the removal efficiencies of REEs/C-4 and REEs/C-8 were superior.

Pyrolysis of dicranopteris pedata powder

TGA analysis was applied to determine the appropriate carbonisation temperature of *Dicranopteris pedata* powder. When the temperature was increased from 30 °C to 1000 °C, two exothermic peaks located at 49.34 and 341.24 °C were observed in the Derivative Thermogravimetry (DTG) curve (Fig. 1b). Indicated here is a significant weight loss by the *Dicranopteris pedata* powder. The complete pyrolysis reaction proceeds were accompanied by decomposition of protein, hemicellulose, cellulose, and lignin[18]. Here the weight loss of *Dicranopteris pedata* powder included three steps. The first stage (< 135 °C) could be attributed to the evaporation of free/bound moisture and a small amount of volatile matter of biomass. The second stage (135–450 °C) was made possible by the elimination of carbohydrates, cellulosic and hemicellulose[19]. The TGA and DTG curves showed that the second stage is the most dominant in the weight loss of *Dicranopteris pedata* powder during calcination and, therefore, the most critical stage in the formation of physicochemical properties of REEs/C. The third and final stage (> 450 °C), due to the evaporation of lignin involved the slow decomposition of lignin and other residues, where the accelerated degradation rate will result in better thermal stability of REEs/C[17,19,20]. Correspondingly, the initial dehydration step observed a 10.12% weight loss. Then, 63.51% of the weight was quickly lost in the decomposition step of biomass, which originated from the pyrolysis of *Dicranopteris pedata* powder. Finally, the weight loss did significantly slow down with 17.41% still remaining at 1000 °C.

Physicochemical property of REEs/C

Crystal structure of the material

XRD was implemented to measure the inner crystalline structure of the three REEs/C. Figure 1c shows the XRD patterns of the three as-prepared REEs/C, where no sharp peaks were observed on any of them, meaning that all materials consisted of amorphous carbon. Compared to REEs/C-4 and REEs/C-8, the higher diffraction peak intensity was found at 22° (002) in the XRD pattern for REEs/C-6. This suggests that REEs/C-6 has a more ordered carbon structure than REEs/C-4, which is attributed to the decomposition of cellulose with higher crystallinity[18]. However, the decomposition process of cellulose can potentially clog the pore structure of REEs/C-6, which may lead to a decrease in the amount of Pb(II) removed[21].

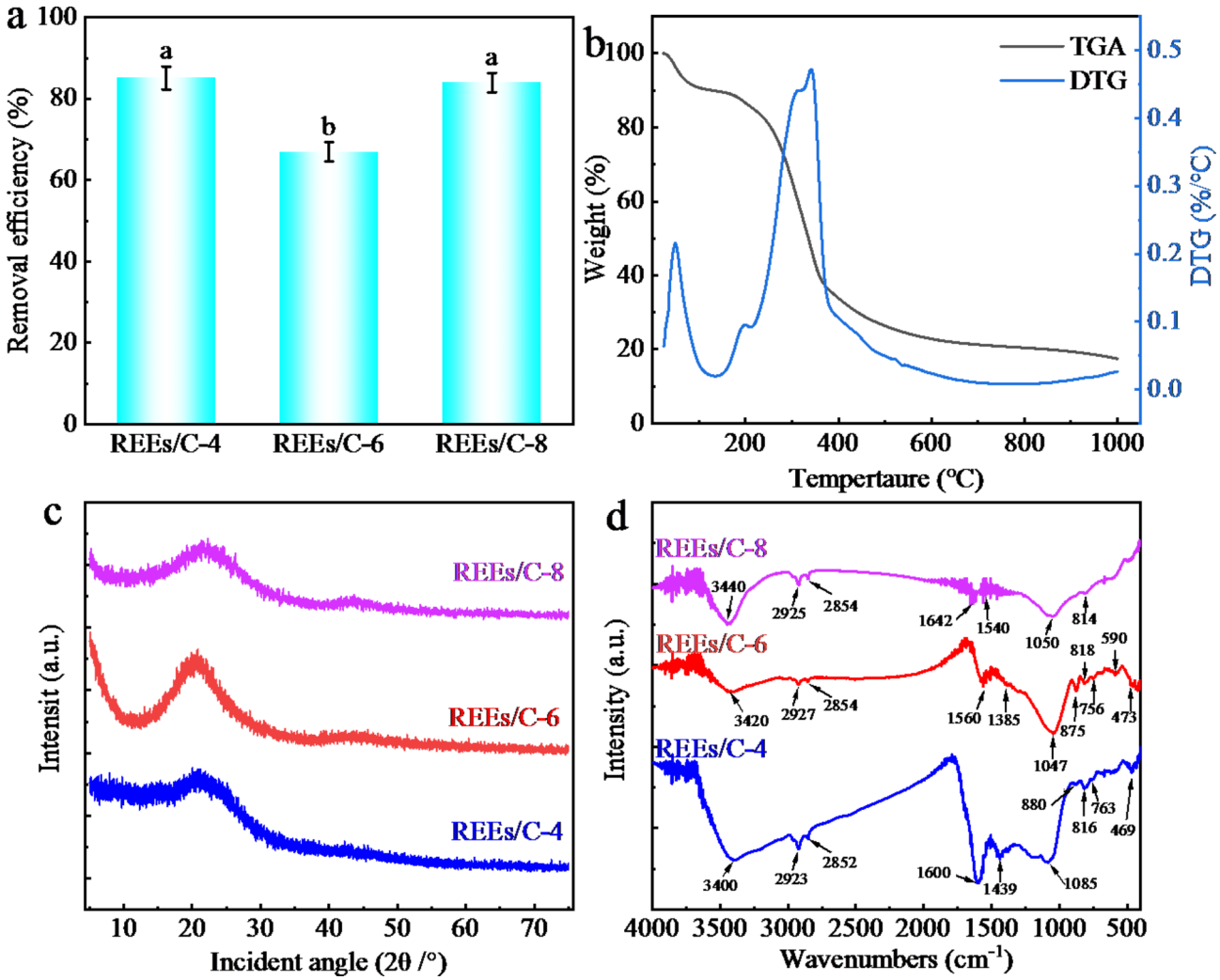

Fig. 1. Removal efficiency of Pb(II) by three carbonisation materials ((**a**) Conditions: dose 1 g·L^{-1}, pH = 5, T = 25 °C, Pb(II) = 15 mg·L^{-1}, n = 3), TGA (**b**) of *Dicranopteris pedata* powder, XRD (**c**) and FTIR (**d**) of REEs/C-4, REEs/C-6, and REEs/C-8. Lowercase letters in Fig. 1a indicate significant differences between treatments, and error bars are standard deviations.

	Surface area (m^2·g^{-1})	Pore volume (cm^3·g^{-1})
REEs/C-4	4.655	0.013
REEs/C-6	1.904	0.012
REEs/C-8	12.745	0.018

Table 2. Surface area and pore volume of the three evaluated REEs/C (n = 3).

Specific surface area and pore structure

The specific surface areas of the three REEs/C were analysed utilising the Brunauer-Emmett-Teller method. As summarised in Table 2, it emerged that the specific surface area of REEs/C-8 was 2.74 times and 6.69 times larger than that of REEs/C-4 and REEs/C-6, respectively. This was possibly caused by the high temperature inducing the calcination of functional groups, thereby forming more pores. Here, the larger surface area of REEs/C-8 will produce more surface-active sites, thereby enhancing Pb(II) removal.

Surface morphology and elements

The surface morphologies of three REEs/C were investigated using SEM. As depicted in Fig. 2a, b, e and f, REEs/C-4 and REEs/C-6, both consisted of irregular rough surfaces with heterogeneous pores and cavities, which was attributed to the decomposition of hemicellulose and cellulose[17]. Nevertheless, the surface of REEs/C-6 was smoother than that of REEs/C-4, which could be explained by the cleavage of cellulose and hemicellulose

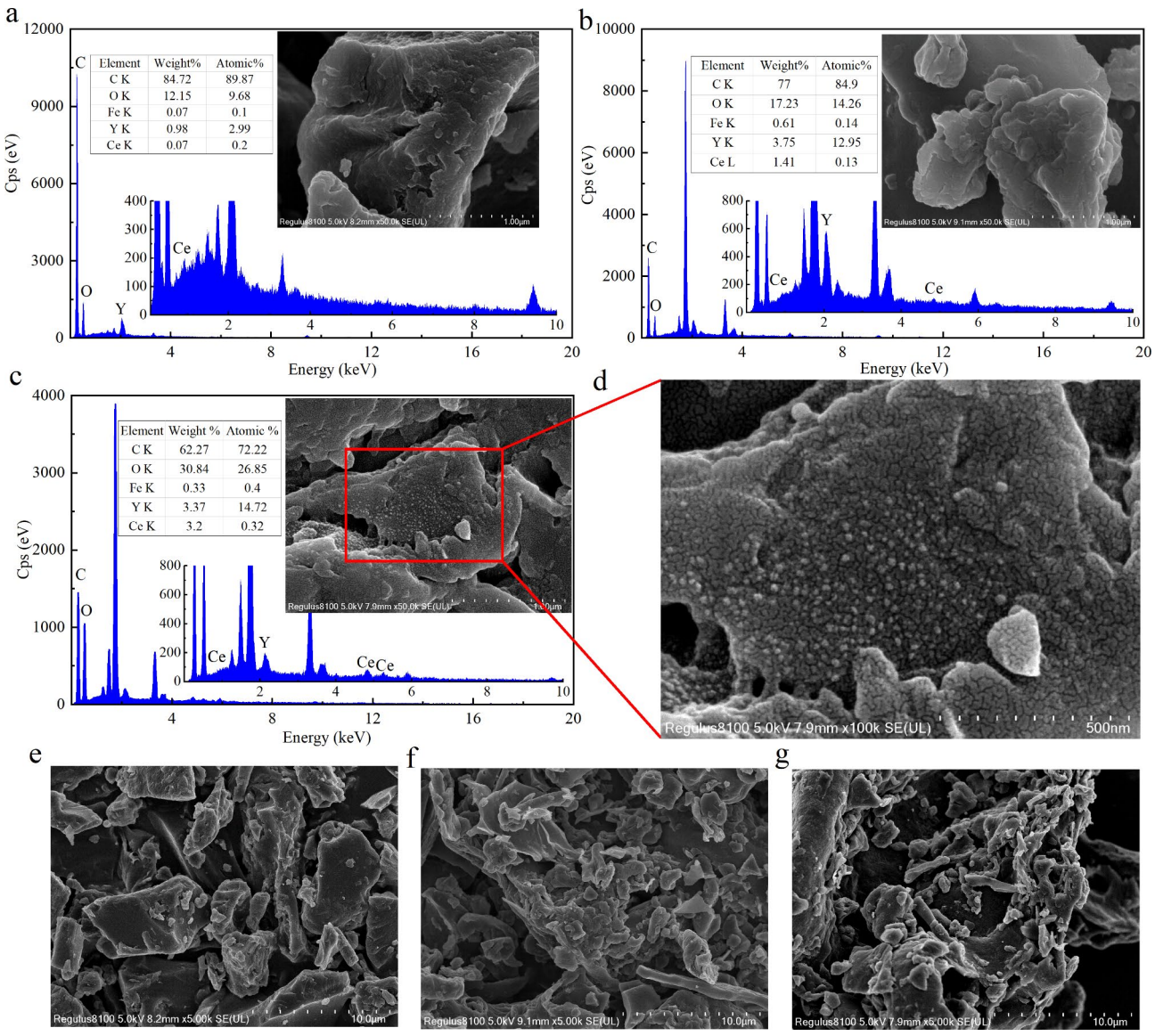

Fig. 2. SEM/EDS of REEs/C-4 (**a**,**e**), REEs/C-6 (**b**,**f**), REEs/C-8 (**c**,**d**,**g**).

leading to a large amount of collapsed structure on REEs/C-6[22]. Compared with REEs/C-4 and REEs/C-6, the surface of REEs/C-8 showed a distinct structure with smaller pores (Fig. 2c, d, and g). Thus, REEs/C-6 had inferior removal capacity due to the decline of specific surface area, while REEs/C-8 possessed superior removal capacity because it had rich pore structures. According to the results of TGA analyses, lignin decomposition was the main reason for the weight loss in the third stage of *Dicranopteris pedata* powder[19,20]. It has been reported that bonded structures, such as benzyl alkyls, aryl ethers, and C-Cs, including β-β, can be cleaved at 700 °C to 800 °C[23]. In addition, at high temperatures, the majority of the aromatic rings were deoxygenated, followed by the production of H_2 due to the rearrangement of the aromatic rings in the polycyclic structure[19]. Thus, it can be concluded that the pore structure on the surface of REEs/C-8 results from the decomposition and volatilisation of volatile substances in lignin. Numerous studies have shown that the charring process leads to the decomposition of volatiles and the eventual formation of pore structures[24,25]. The results of BET were strong evidence that the pore structure of REEs/C-8 is superior to that of REEs/C-40 and REEs/C-6.

EDS showed that the relative content of C decreased and that of O increased with increasing charring temperature, contrary to the results of previous studies. It is noteworthy that REEs bind to biomolecules such as hemicellulose, cellulose, lignin, and organic acids in plants in an ionic form[26,27]. Accordingly, and in conjunction with the results of the TGA, it is known that endogenous REEs were released from *Dicranopteris pedata* powder during calcination due to the charring of lignin, hemicellulose, and cellulose. At the same time, oxygen-containing compounds in the *Dicranopteris pedata* powder were decomposed and volatilised during charring, releasing the O element[23]. Rare earth oxides are highly thermally stable[28]. Consequently, a large number of REEs in the *Dicranopteris pedata* powder reacted with elemental O during calcination to form rare earth oxides, retaining elemental O in the REEs/C. This is an important reason for the increase in the

relative content of O in REEs/C with the increase in calcination temperature. Moreover, Y and Ce were both observed on the REEs/C surface, where the weight and atomic percentages of both clearly rose with an increase in calcination temperature. Doping with REEs can alter the ionic coordination of the carbonisation material, reducing the surface electronegativity and decreasing electrostatic repulsion, thereby improving pollutant removal[29]. For example, La-modified pineapple peel charred material increased adsorption capacity by about 27 times[30]. Therefore, the REEs also had the function in the REEs/C to enhance the adsorption capacity of material. Accordingly, the elevation in REEs content can change the ionic coordination of the carbonisation material and reduce surface electronegativity, thus improving the removal performance of REEs/C-8[29].

Surface functional group

FTIR spectra were employed to detect functional groups on different REEs/C surfaces[23]. As shown in Fig. 1d, REEs/C-4 exhibited abundant functional groups, such as aromatic CH (816 cm^{-1}), C-O stretching vibration of phenolic or ester groups (1085 cm^{-1}), CH_2 (2923 and 1439 cm^{-1}), aromatic C = C and C = O stretching vibration (1600 cm^{-1}) and hydroxyl (-OH) groups stretching vibration (3400 cm^{-1}). These wealthy functional groups can function as chelation sites to effectively bind with Pb(II). As well, the functional groups in REEs/C-6 significantly diminished when the calcination temperature increased[18,23], thus leading to a reduction in the removal capacity. Similar findings regarding the reduction in the type or content of surface functional groups have been reported by Hwang et al.[23], Chu et al.[31] and Ma et al.[18]. This phenomenon was attributed to the decomposition of lignin, cellulose and hemicellulose-related compounds into volatiles such as H_2, CO, CO_2, H_2O, and tars[32], resulting in the decomposition of many functional groups from the carbonisation material during carbonisation of *Dicranopteris pedata* powder. It has been reported that the vibrations in the frequency range 700–1200 cm^{-1} and 1200–2000 cm^{-1} are considered aliphatic and aromatic nature of materials, respectively[24]. Notably, the aliphatic organic compounds (400–1000 cm^{-1}) present in REEs/C-8 transformed into aromatic organic compounds during heat treatment[19,33]. Since the presence of an aromatic structure could facilitate the interaction between adsorbents and contaminants[25], the superior removal performance of REEs/C-8 was obtained.

Morphology of chemical elements on the surface of the material

XPS analysis was undertaken to observe the changes in surface chemical compositions and chemical state of the three REEs/C. As shown in Fig. 3a, C 1s spectra revealed the C content of REEs/C-8 was 1.37 and 1.32 times larger than that of REEs/C-4 and REEs/C-6, respectively, confirming the complete carbonisation of hemicellulose, cellulose, and lignin at 800 °C. Three peaks appeared at 284.8, 285.7, and 289.3 eV, corresponding to the C-C/C = C, C-O (phenol and alcohol), and O = C-O (carbonyl) groups, respectively[34]. Here, the proportions of C-C/C = C groups in REEs/C-8 achieved 76.06% relative to REEs/C-4 (64.91%) and REEs/C-6 (73.73%). This occurred because the unstable carbon-oxygen bonding can be easily converted to a stable C = C structure by polycyclization[23]. These outcomes further confirmed the generation of aromatisation carbon structure after calcination[23,35].

As given in Fig. 3b, the O 1s spectra of the three evaluated REEs/C showed three peaks attributable to C = O (531.6 eV), O-C = O (532.6 eV), and C-O groups (533.8 eV), respectively[34]. Notably, the appearance of the peak at 530.7 eV demonstrated the generation of REEs-O-C[36]. As the calcination temperature rose, the relative peak intensities attributable to the metallic oxide also gradually increased. Here, the proportion of metallic oxide in REEs/C-8 was 17.81%, while only 15.57% and 10.24% were obtained in REEs/C-4 and REEs/C-6, respectively. This probably was due to the appearance of oxygen vacancies and C-O-Ce bond in REEs/C-8[37]. The study by Zheng et al.37 reported that the oxygen vacancies formed on the surface of CeO can enhance the adsorption capacity of the material. Therefore, we judge that REEs/C-8 has a stronger Pb removal ability due to creating more oxygen vacancies in the material.

To prove the existence of REEs in REEs-C, XPS spectra of the Y 3d and Ce 3d were investigated. As illustrated in Fig. 3c, the deconvolution of the Y $3d_{5/2}$ spectra indicated yttrium metal ions present on the REEs-C surface[38]. Furthermore, the Ce 3d spectra could be deconvoluted two chemical components, namely Ce(III) and Ce(IV) (Fig. 3d). The peaks at 880.4, 899.1, 885.0, and 903.2 eV belong to Ce(III), while the other peaks at 882.4, 900.9, 889.0, 907.3, 898.3, and 916.7 eV were attributed to Ce(IV)[39]. Additionally, the peak intensities of Ce(III) fell from 50.34 to 35.07% with an increase in calcination temperature, which suggested that Ce(III) was oxidised to Ce(IV) during the calcination process[40]. This provides strong evidence that Ce causes the appearance of more oxygen vacancies in REEs/C-8.

In summary, the XPS characterisation results demonstrate that REEs/C-8 possesses a stronger Pb(II) removal capacity, which is attributed to the formation of more aromatic structures, rare earth oxides and oxygen vacancies during the charring process.

Zeta potential

To investigate the surface charge of the three REEs/C, their zeta potential was measured in the pH range of 4–10. As displayed in Fig. 4, it can be observed that all REEs/C have an isoelectric point at pH 5. As well, the zeta potential of REEs/C was mainly positive at pH < 5 and negative at pH > 5. According to the one-way ANOVA, the zeta potential of the three REEs/C was significantly different at pH 4, 5, 7, 8, and 9 ($P < 0.05$). The REEs/C-8 possessed more negative charges in the pH range of 5–9 relative to REEs/C-4 ($P < 0.05$). Calcination caused the reduction of functional groups, electrically neutralising a fraction of the REEs/C surface, thus causing electrostatic attraction between Pb(II) and REEs/C-6 to weaken. Nevertheless, the negative charge on the REEs/C-8 surface helped to enhance the electrostatic attraction, hence improving the removal performance of REEs/C-8[41]. Therefore, surface electronegative charges of REEs/C-8 could increase Pb(II) adsorption through electrostatic interaction. This is one of the reasons for the REEs/C-8 better efficiency in removing Pb(II).

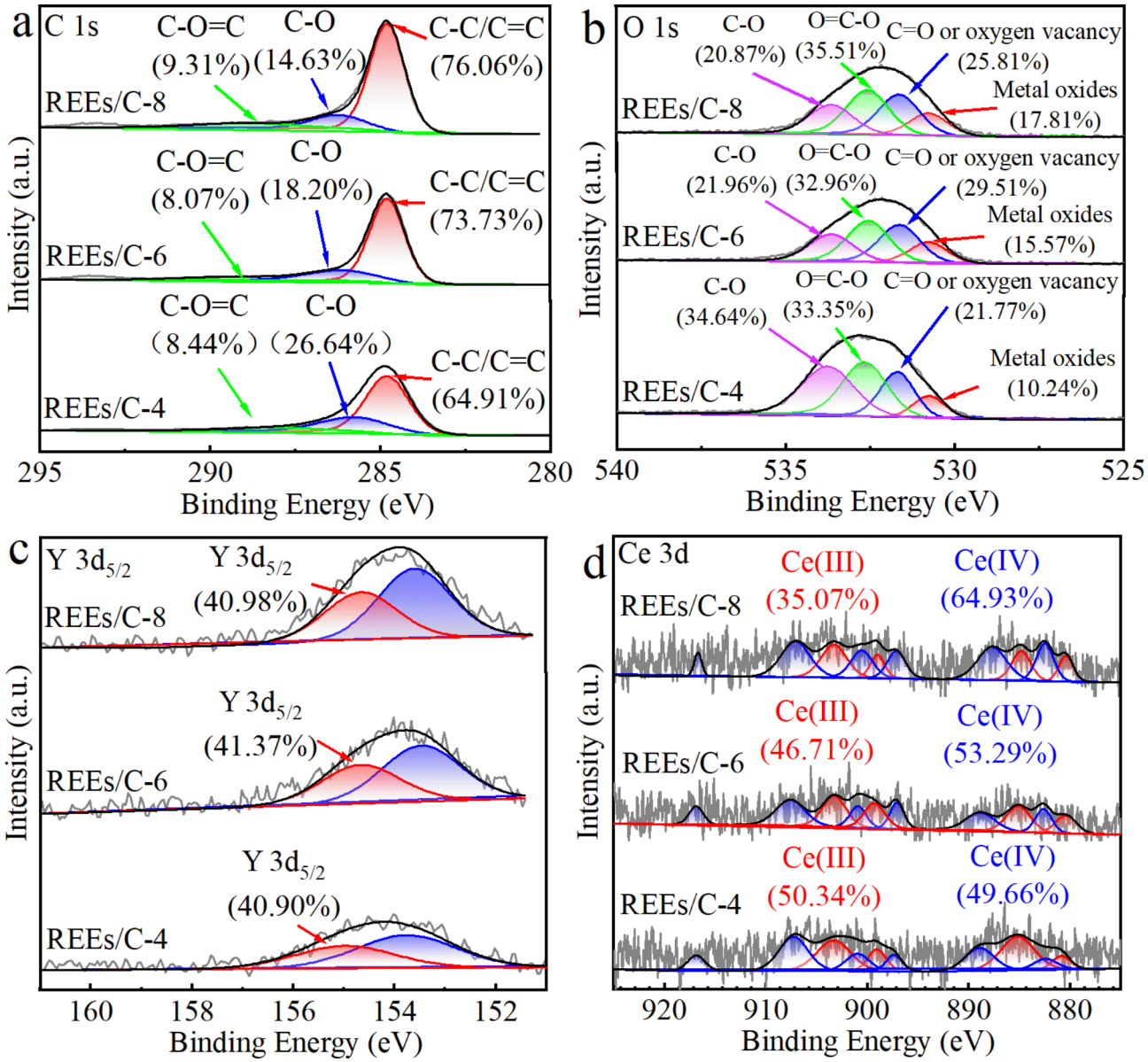

Fig. 3. XPS spectra of three REEs/C: (**a**) C 1s, (**b**) O 1s, (**c**) Y $3d_{5/2}$, (**d**) Ce 3d.

Adsorption kinetics and thermodynamics

The results of fitting the adsorption model are shown in Figs. 5 and 6; Table 3. The R^2 values of the pseudo-second-order kinetic model were generally higher than those of the pseudo-first-order model. Therefore, the pseudo-second-order kinetic model better described the adsorption of Pb(II) by all three REEs/Cs, implying that chemical interactions were involved per the model's assumptions[15]. This is consistent with the FTIR and XPS results, which indicated that surface functional groups of the material adsorb Pb(II) via ion exchange and chelation. The high α value and low β value of the Elovich model for Pb(II) adsorption suggested a rapid initial adsorption rate that decreases as surface sites become occupied[42]. Therefore, REEs/C-8 with better pore structure had the fastest adsorption rate and thus possess the strongest Pb(II) removal capacity. Furthermore, the fitting results of our intraparticle diffusion model showed that none of the model straight lines passed through the origin of the coordinate axis, and all fitted to three straight lines. This suggested that the adsorption processes by REEs/Cs were controlled by multiple diffusion mechanisms[43]. The intraparticle diffusion model also showed that the adsorption process of Pb(II) by REEs/Cs could all be divided into three stages: an initial rapid adsorption dominated by liquid film diffusion, an intraparticle diffusion stage dominated by internal pore diffusion, and an equilibrium stage dominated by slow micropore diffusion. This indicated that the boundary layer effect gradually increases with adsorption time, becoming the main limiting factor in the Pb(II) adsorption process by REEs/Cs[44]. The R^2 values of the Langmuir model for Pb(II) removal were higher than those of the Freundlich model, indicating that the Langmuir model better described the adsorption process of REEs/C on Pb(II). Thus, the adsorption sites on REEs/C were uniformly distributed on its surface, and ion exchange played a significant

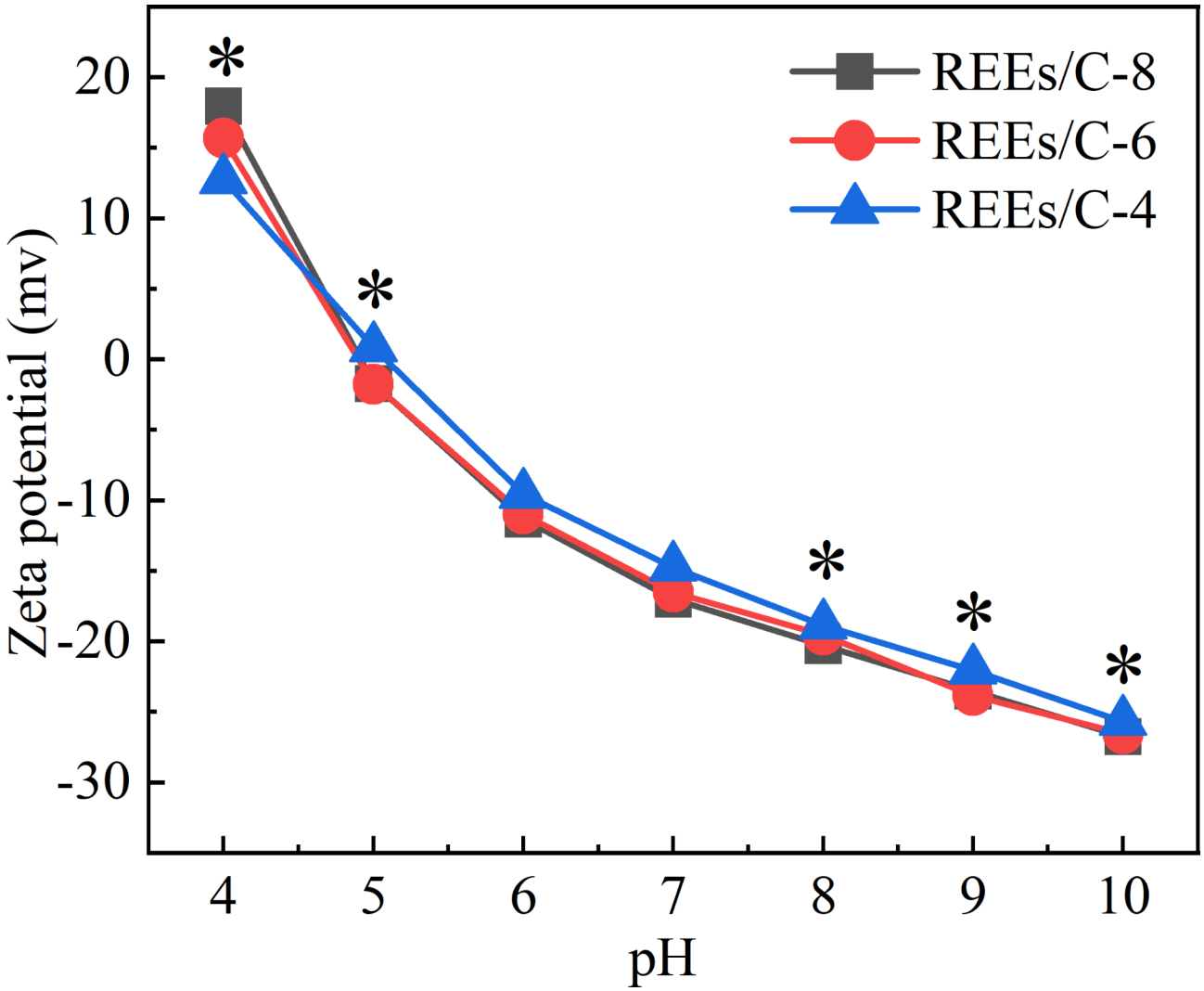

Fig. 4. Zeta potential at different pH levels of the three tested REEs/C ($n = 3$). *Represents significant differences in the zeta potential of the REEs/Cs.

role[45]. According to the q_{max} parameter of the Langmuir model, the maximum adsorption capacity could reach 74.79 $mg \cdot g^{-1}$ at 25 °C and increase with rising reaction temperature. Thermodynamic calculations revealed that the adsorption of Pb(II) by REEs/C was a spontaneous and highly disordered process[46]。.

Leaching of material endogenous REEs during adsorption

To assess the possible environmental risk caused by the leaching of endogenous REEs from REEs/C during Pb removal, we examined the concentration of REEs in solution after the removal experiments (Table 4). The total concentration of REEs in the solution was extremely low. This indicates that the REEs/C prepared at the three temperatures had minimal leaching of REEs during Pb removal. Therefore, we conclude that REEs/C is a safe and environmentally friendly adsorbent.

Application in wastewater

The above three as-prepared REEs/C showed high activity for removing Pb(II) in a spiked wastewater sample, achieving the removal efficiencies of 88.5 to 94.0% (Fig. 7). This suggested that the wastewater had, in terms of Pb(II), at least been successfully remediated. More importantly, the evaluated REEs/C have great potential for the practical remediation of wastewater containing elevated Pb(II) levels. This work creatively prepared *Dicranopteris pedata*, a hyperaccumulator that extracted REEs from mining areas, into a functional carbonisation material with great potential for remediation of heavy metal pollution. This is a key part of the remediation of the ecological environment in rare earth mining areas using *Dicranopteris pedata*, which provides novel ideas and technologies to promote the sustainable development of the rare earth industry.

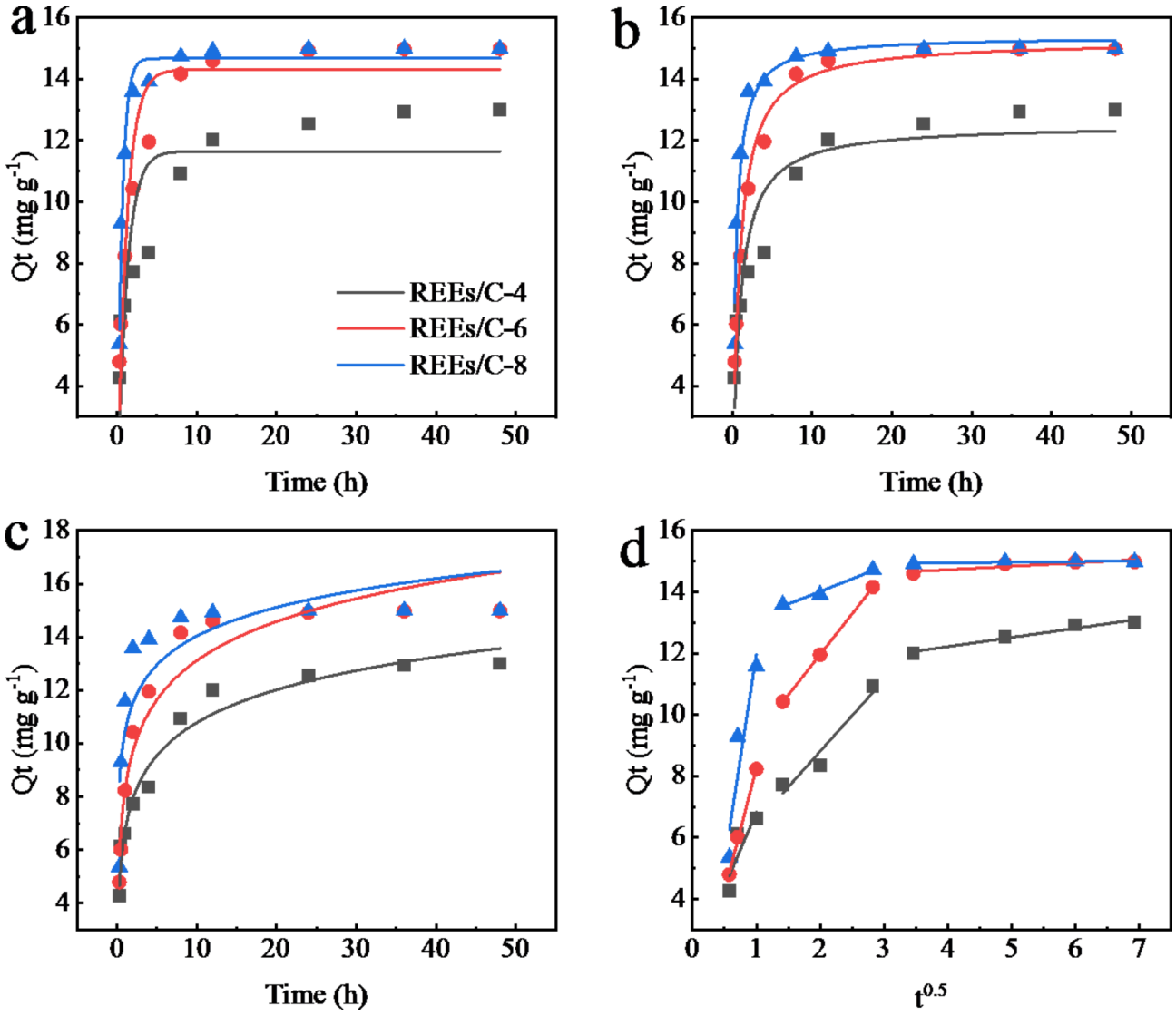

Fig. 5. Pseudo-first-order kinetics (**a**), pseudo-second-order kinetics (**b**), Elovich kinetics (**c**) and intraparticle diffusion model (**d**) for Pb(II) removal by REEs/Cs ($n = 3$).

Conclusions

In this study, the structure-activity relationship of the three REEs-C (REEs/C-4, REEs/C-6, and REEs/C-8) was demonstrated. REEs/C-4 exhibited strong Pb(II) removal capability due to its superior surface pore structure, larger specific surface area, and abundant functional groups. As the calcination temperature increased, the functional groups in REEs/C-6 diminished significantly and the collapse of the carbon structure blocked the pore structure. Thus, the removal ability of REEs/C-6 was weakened. As well, high temperature calcination enabled REEs/C-8 to engage in complete aromatization, have a richer pore structure, higher REEs concentration and stronger electrostatic attraction, resulting in the most outstanding Pb(II) removal capacity. The fitting results of the adsorption model also confirmed that chemisorption, such as ion exchange and chelation, played a key role. In terms of the whole adsorption process, the adsorption of Pb(II) by REEs/C was a spontaneous and strongly disordered adsorption process. Hence, *Dicranopteris pedata* clipping extracted with REEs from mine soil was successfully transformed into endogenous rare earth carbonisation materials with great Pb(II) removal potential. This method avoided the risk of secondary contamination and successfully reused the *Dicranopteris pedata* clippings in a resource manner. Our work supports the application of phytoremediation to the ecological restoration of rare earth mining sites and provides a sound basis for future scientific research. In addition, REEs are of extraordinary value as critical raw materials for high-tech industries. Therefore, it is significant to recover REEs from *Dicranopteris pedata* carbonisation materials, which will become one of our key focus areas in the future.

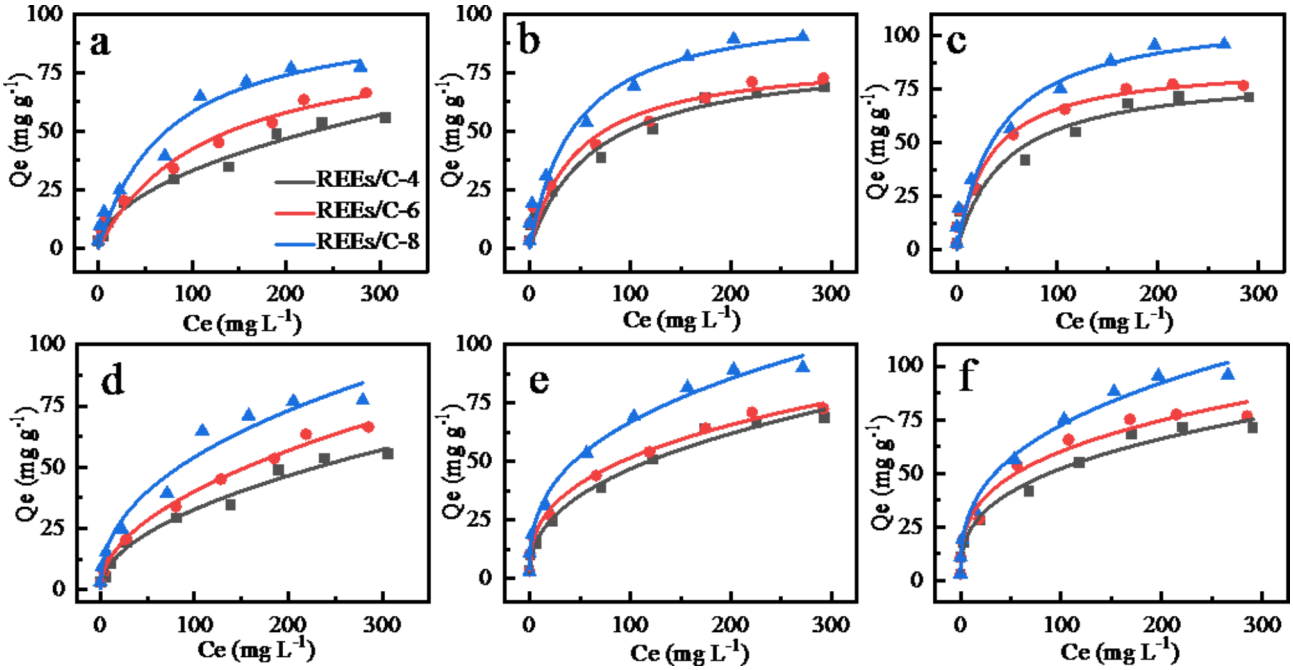

Fig. 6. Langmuir for REEs/C-4 (**a**), REEs/C-6 (**b**) and REEs/C-8 (**c**) and Freundlich for REEs/C-4 (**d**), REEs/C-6 (**e**) and REEs/C-8 (**f**) with Pb(II) removal ($n = 3$).

Model		Parameters	REEs/C-4			REEs/C-6			REEs/C-8		
Pseudo-first order		Q_e (mg g^{-1})	11.64			14.30			14.67		
		K_1 (min^{-1})	0.85			0.85			1.69		
		R^2	0.75			0.93			0.97		
Pseudo-second order		Q_e (mg g^{-1})	12.52			15.26			15.39		
		K_2 (g (mg·min)$^{-1}$)	0.09			0.08			0.17		
		R^2	0.90			0.99			0.97		
Elovich		a (mg g^{-1} s^{-1})	75.17			101.42			125.24		
		b	0.56			0.47			0.64		
		R^2	0.97			0.93			0.86		
Intramaterial diffusion	External surface sorption	K_{int1} (g mg^{-1} $min^{-0.5}$)	4.88			8.05			13.52		
		C_1	1.94			0.22			-1.55		
		R^2	0.74			0.99			0.87		
	Gradual adsorption	K_{int2} (g mg^{-1} $min^{-0.5}$)	2.32			2.64			0.82		
		C_2	4.16			6.68			12.37		
		R^2	0.94			0.99			0.98		
	Final equilibrium	K_{int3} (g mg^{-1} $min^{-0.5}$)	0.30			0.11			0.02		
		C_2	11.03			14.28			14.86		
		R^2	0.96			0.81			0.90		
			25 °C	35 °C	45 °C	25 °C	35 °C	45 °C	25 °C	35 °C	45 °C
Langmuir		q_{max} (mg g^{-1})	74.79	91.85	101.36	73.48	82.20	104.73	82.74	87.23	110.80
		K_L (L mg^{-1})	0.01	0.01	0.01	0.02	0.02	0.02	0.02	0.03	0.02
		R^2	0.97	0.97	0.96	0.96	0.95	0.96	0.94	0.96	0.96
Freundlich		K_F ($mg^{1-n}L^n$ g^{-1})	3.15	3.99	7.37	7.31	10.40	13.09	10.85	14.37	14.69
		1/n	−1.97	−1.99	−2.31	−2.48	−2.87	−2.82	−2.93	−3.21	−2.88
		R^2	0.98	0.99	0.97	0.99	0.99	0.99	0.98	0.98	0.99
Thermodynamics		△G° (KJ mol^{-1})	−0.12			−5.23			−9.63		
		△H° (KJ mol^{-1})	69.14			64.78			20.09		
		△S° (J $molK^{-1}$)	231.79			236.40			99.32		
		R^2	0.99			0.87			0.90		

Table 3. The modal parameters for pb(II) adsorbed on three carbonisation materials ($n = 3$).

	REEs/C-4	REEs/C-6	REEs/C-8		REEs/C-4	REEs/C-6	REEs/C-8
Sc	0.000	0.000	0.019	Gd	0.000	0.000	0.001
Y	0.004	0.007	0.026	Tb	0.000	0.000	0.000
La	0.005	0.002	0.006	Dy	0.001	0.002	0.001
Ce	0.000	0.000	0.002	Ho	0.000	0.000	0.000
Pr	0.004	0.002	0.004	Er	0.001	0.002	0.001
Nd	0.009	0.005	0.004	Tm	0.000	0.000	0.000
Sm	0.000	0.000	0.002	Yb	0.000	0.000	0.000
Eu	0.000	0.000	0.001	Lu	0.000	0.000	0.000

Table 4. Content of REEs in solution after adsorption of pb by REEs/C ($n = 3$, mg L^{-1}).

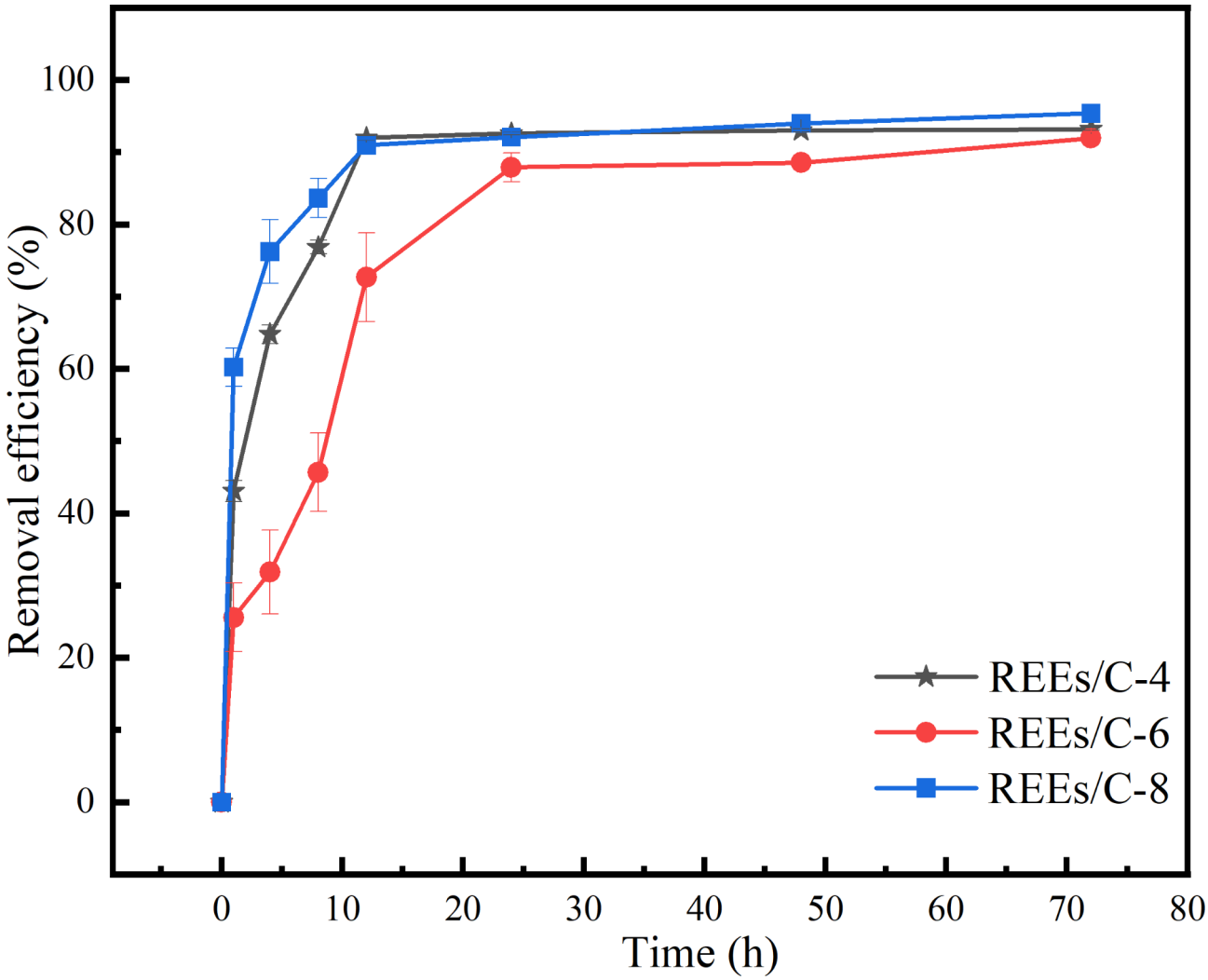

Fig. 7. The removal efficiency of Pb(II) by three tested REEs/C in wastewater samples ($n = 3$). The error bars in the graphs are standard deviations.

Data availability

Data is provided within the manuscript or supplementary information files.

Received: 1 October 2024; Accepted: 8 January 2025
Published online: 22 February 2025

References

1. Li, X. F., Chen, Z. B., Chen, Z. Q. & Zhang, Y. H. A human health risk assessment of rare earth elements in soil and vegetables from a mining area in Fujian Province, Southeast China. *Chemosphere* **93**, 1240–1246. https://doi.org/10.1016/j.chemosphere.2013.06.085 (2013).
2. Wu, J. L., Chen, A. Q., Peng, S. L., Wei, Z. G. & Liu, G. C. Identification and application of amino acids as chelators in phytoremediation of rare earth elements lanthanum and yttrium. *Plant. Soil.* **373**, 329–338. https://doi.org/10.1007/s11104-013-1811-0 (2013).
3. Wang, L., Ji, B., Hu, Y. H., Liu, R. Q. & Sun, W. A review on in situ phytoremediation of mine tailings. *Chemosphere* **184**, 594–600. https://doi.org/10.1016/j.chemosphere.2017.06.025 (2017).
4. Chen, Z. Q., Chen, Z. B., Yan, X. Y. & Bai, L. Y. Stoichiometric mechanisms of *Dicranopteris dichotoma* growth and resistance to nutrient limitation in the Zhuxi watershed in the red soil hilly region of China. *Plant. Soil.* **398**, 367–379. https://doi.org/10.1007/s11104-015-2670-7 (2016).
5. Yang, L. et al. Rethinking the ecosystem functions of Dicranopteris, a widespread Genus of ferns. *Front. Plant. Sci.* **11**, 581513. https://doi.org/10.3389/fpls.2020.581513 (2021).
6. Wei, Z. G. et al. Subcellular and molecular localization of rare earth elements and structural characterization of yttrium bound chlorophyll in naturally grown fern. *Microchem J.* **80**, 1–8. https://doi.org/10.1016/j.microc.2004.07.005 (2005).
7. Yan, S. P. et al. Hyperaccumulator extracts promoting the phytoremediation of rare earth elements (REEs) by Phytolacca americana: role of active microbial community in rhizosphere hotspots. *Environ. Res.* **252**. https://doi.org/10.1016/j.envres.2024.118939 (2024).

8. Chen, Z. Q., Chen, Z. B. & Bai, L. Y. Rare earth element migration in gullies with different *Dicranopteris dichotoma* covers in the Huangnikeng gully group, Changting County, Southeast China. *Chemosphere* **164**, 443–450. https://doi.org/10.1016/j.chemosphere.2016.08.123 (2016).
9. Zheng, H. X. et al. Rare earth elements detoxification mechanism in the hyperaccumulator Dicranopteris linearis: [silicon-pectin] matrix fixation. *J. Hazard. Mater.* **452** https://doi.org/10.1016/j.jhazmat.2023.131254 (2023).
10. Ma, S. R. et al. Mowing improves chromium phytoremediation in *Leersia hexandra* Swartz. *Sustainability* **15**, 15076244. https://doi.org/10.3390/su15076244 (2023).
11. Chen, Z. Q., Chen, Z. B. A., Feng, L. J. & Yang, M. G. Rare earth element migration and impact of Dicranopteris dichotoma at mines in south China. *Chemosphere* **278**, 130433. https://doi.org/10.1016/j.chemosphere.2021.130433 (2021).
12. Chen, Z. & Chen, Z. Clipping strategy to assist phytoremediation by hyperaccumulator *Dicranopteris dichotoma* at rare earth mines. *Int. J. Phytoremediat* **22**, 1038–1047. https://doi.org/10.1080/15226514.2020.1725870 (2020).
13. Wang, L. et al. Development of rare earth element doped magnetic biochars with enhanced phosphate adsorption performance. *Colloid Surf. A* **561**, 236–243. https://doi.org/10.1016/j.colsurfa.2018.10.082 (2019).
14. Bhuvanendran, N. et al. Spindle-shaped CeO2/biochar carbon with oxygen-vacancy as an effective and highly durable electrocatalyst for oxygen reduction reaction. *Int. J. Hydrogen Energ.* **46**, 2128–2142. https://doi.org/10.1016/j.ijhydene.2020.10.115 (2021).
15. Sun, T. et al. Crayfish shell biochar for the mitigation of pb contaminated water and soil: characteristics, mechanisms, and applications. *Environ. Pollut* **271**, 116308. ARTN 11630810.1016/j.envpol.2020.116308 (2021).
16. Wu, F. F. et al. Industrial alkali lignin-derived biochar as highly efficient and low-cost adsorption material for pb(II) from aquatic environment. *Bioresource Technol.* **322**, 124539. https://doi.org/10.1016/j.biortech.2020.124539 (2021).
17. Mallick, D., Poddar, M. K., Mahanta, P. & Moholkar, V. S. Discernment of synergism in pyrolysis of biomass blends using thermogravimetric analysis. *Bioresource Technol.* **261**, 294–305. https://doi.org/10.1016/j.biortech.2018.04.011 (2018).
18. Ma, Q. L. et al. Physicochemical properties of biochar derived from anaerobically digested dairy manure. *Waste Manag.* **79**, 729–734. https://doi.org/10.1016/j.wasman.2018.08.023 (2018).
19. Mishra, R. K. & Mohanty, K. Pyrolysis kinetics and thermal behavior of waste sawdust biomass using thermogravimetric analysis. *Bioresource Technol.* **251**, 63–74. https://doi.org/10.1016/j.biortech.2017.12.029 (2018).
20. Reza, M. S. et al. Biochar characterization of invasive *Pennisetum purpureum* grass: effect of pyrolysis temperature. *Biochar* **2**, 239–251. https://doi.org/10.1007/s42773-020-00048-0 (2020).
21. Song, X. et al. Surface characterization studies of walnut-shell biochar catalysts for simultaneously removing of organic sulfur from yellow phosphorus tail gas. *Appl. Surf. Sci.* **425**, 130–140. https://doi.org/10.1016/j.apsusc.2017.06.328 (2017).
22. Rosa, J. M., Paneque, M., Miller, A. Z. & Knicker, H. Relating physical and chemical properties of four different biochars and their application rate to biomass production of Lolium perenne on a calcic cambisol during a pot experiment of 79 days. *Sci. Total Environ.* **499**, 175–184. https://doi.org/10.1016/j.scitotenv.2014.08.025 (2014).
23. Hwang, H., Ajaz, A. M. & Choi, J. W. A study on activation mechanism in perspective of lignin structures and applicability of lignin-derived activated carbons for pollutant absorbent and supercapacitor electrode. *Chemosphere* **291**, 133045. https://doi.org/10.1016/j.chemosphere.2021.133045 (2022).
24. Muktham, R., Ball, A. S., Bhargava, S. K. & Bankupalli, S. Study of thermal behavior of deoiled karanja seed cake biomass: thermogravimetric analysis and pyrolysis kinetics. *Energy Sci. Eng.* **4**, 86–95. https://doi.org/10.1002/ese3.109 (2016).
25. Viswanthan, S. P. et al. Removal efficiency of methylene blue from aqueous medium using biochar derived from *Phragmites karka*, a highly invasive wetland weed. *Biomass Convers. Bior* **12**, 3257–3273. https://doi.org/10.1007/s13399-020-00877-w (2022).
26. Zhang, L. et al. Revegetation of a barren rare earth mine using native plant species in reciprocal plantation: effect of phytoremediation on soil microbiological communities. *Environ. Sci. Pollut R* **27**, 2107–2119. https://doi.org/10.1007/s11356-019-06645-2 (2020).
27. Liu, C. et al. The limited exclusion and efficient translocation mediated by organic acids contribute to rare earth element hyperaccumulation in *Phytolacca americana*. *Sci. Total Environ.* **805**, 150335. https://doi.org/10.1016/j.scitotenv.2021.150335 (2022).
28. Velmuzhov, A. P. et al. Rare-earth metals as effective getters for purification of germanium telluride glasses from oxygen impurities. *J. Non-Cryst Solids* **603**, 122112. https://doi.org/10.1016/j.jnoncrysol.2022.122112 (2023).
29. Li, S. et al. Remediation of nitrate contaminated groundwater using a simulated PRB system with an La-CTAC-modified biochar filler. *Front. Env Sci-Switz* **10**, 986866. https://doi.org/10.3389/fenvs.2022.986866 (2022).
30. Liao, T. W. et al. La(OH)3-modified magnetic pineapple biochar as novel adsorbents for efficient phosphate removal. *Bioresource Technol.* **263**, 207–213. https://doi.org/10.1016/j.biortech.2018.04.108 (2018).
31. Chu, G. et al. Phosphoric acid pretreatment enhances the specific surface areas of biochars by generation of micropores. *Environ. Pollut.* **240**, 1–9. https://doi.org/10.1016/j.envpol.2018.04.003 (2018).
32. Vikraman, V. K., Kumar, D. P., Boopathi, G. & Subramanian, P. Kinetic and thermodynamic study of finger millet straw pyrolysis through thermogravimetric analysis. *Bioresource Technol.* **342**, 125992. https://doi.org/10.1016/j.biortech.2021.125992 (2021).
33. Karakaş, C., Özçimen, D. & İnan, B. Potential use of olive stone biochar as a hydroponic growing medium. *J. Anal. Appl. Pyrol.* **125**, 17–23. https://doi.org/10.1016/j.jaap.2017.05.005 (2017).
34. Liu, N. et al. Removal mechanisms of aqueous cr(VI) using apple wood biochar: a spectroscopic study. *J. Hazard. Mater.* **384**, 121371. https://doi.org/10.1016/j.jhazmat.2019.121371 (2020).
35. Qu, J. H. et al. Green synthesis of hydrophilic activated carbon supported sulfide nZVI for enhanced pb(II) scavenging from water: characterization, kinetics, isotherms and mechanisms. *J. Hazard. Mater.* **403**, 123607. https://doi.org/10.1016/j.jhazmat.2020.123607 (2021).
36. Ouyang, D. et al. Degradation of 1,4-dioxane by biochar supported nano magnetite particles activating persulfate. *Chemosphere* **184**, 609–617. https://doi.org/10.1016/j.chemosphere.2017.05.156 (2017).
37. Zheng, X. Y., Hu, L. F., Zhu, J. C., He, J. & Liu, X. J. Effect of the dispersion behavior of cerium oxygen species on CO2 adsorption performance. *J. Environ. Chem. Eng.* **10**, 106986. https://doi.org/10.1016/j.jece.2021.106986 (2022).
38. Arevalo-Lopez, E. P. et al. Effect of Y-doped NbB2.5 on structural and superconducting properties. *Phys. Scripta* **96**, 065805. https://doi.org/10.1088/1402-4896/abf068 (2021).
39. Dawkins, K., Rudyk, B. W., Xu, Z. & Cadien, K. The pH-dependant attachment of ceria nanoparticles to silica using surface analytical techniques. *Appl. Surf. Sci.* **345**, 249–255. https://doi.org/10.1016/j.apsusc.2015.03.170 (2015).
40. Wang, Y., Xie, X. M., Chen, X. L., Huang, C. H. & Yang, S. Biochar-loaded $Ce3^{+}$-enriched ultra-fine ceria nanoparticles for phosphate adsorption. *J. Hazard. Mater.* **396**, 122626. https://doi.org/10.1016/j.jhazmat.2020.122626 (2020).
41. Bashir, S., Zhu, J., Fu, Q. & Hu, H. Comparing the adsorption mechanism of cd by rice straw pristine and KOH-modified biochar. *Environ. Sci. Pollut R* **25**, 11875–11883. https://doi.org/10.1007/s11356-018-1292-z (2018).
42. Jiang, W., Cai, Y., Liu, D., Yu, X. & Wang, Q. Enhanced adsorption performance of oxytetracycline in aqueous solutions by Mg-Fe modified suaeda-based magnetic biochar. *Environ. Res.* **241**, 117662. https://doi.org/10.1016/j.envres.2023.117662 (2024).
43. Zhang, N., Reguyal, F., Praneeth, S. & Sarmah, A. K. A novel green synthesized magnetic biochar from white tea residue for the removal of pb(II) and cd(II) from aqueous solution: regeneration and sorption mechanism. *Environ. Pollut* **330**, 121806. https://doi.org/10.1016/j.envpol.2023.121806 (2023).
44. Hu, H., Gao, M., Wang, T. & Jiang, L. Efficient uranium adsorption and mineralization recycle by nano-MgO biochar with super-hydrophilic surface. *J. Environ. Chem. Eng.* **11**. https://doi.org/10.1016/j.jece.2023.110542 (2023).
45. Nejad, M. S. & Sheibani, H. Super-efficient removal of arsenic and mercury ions from wastewater by nanoporous biochar-supported poly 2-aminothiophenol. *J. Environ. Chem. Eng.* **10**. https://doi.org/10.1016/j.jece.2022.107363 (2022).

46. Zhang, Y., Yue, X., Xu, W., Zhang, H. & Li, F. Amino modification of rice straw-derived biochar for enhancing its cadmium (II) ions adsorption from water. *J. Hazard. Mater.* **379**, 120783. https://doi.org/10.1016/j.jhazmat.2019.120783 (2019).

Acknowledgements
Funding by the National Natural Science Foundation of China (No. 42277013), the Program for Cultivating Innovative Team, Fujian Normal University (Y0720409B06), Natural Science Foundation of Fujian Province (No. 2020J01143), Science and Technology Project of Water Resources Department of Fujian Province (MSK202201), and Science and Technology Project of Water Resources Department of Fujian Province (MSK202435) are gratefully acknowledged.

Author contributions
Liujun Feng: Roles/Writing - original draft, Investigation, Methodology, Software, Data curation and analysis Writing - review & editing.Zhiqiang Chen: Conceptualization, Data curation, Funding acquisition, Methodology, Project administration, Writing - review & editing.Haiyan Wang: Investigation, Methodology, Formal analysis, Data curation and analysis.Zhibiao Chen: Funding acquisition, Project administration, Writing - review & editing.Zuliang Chen: Conceptualization, Writing - review & editing.Jianhua Liu: Writing - review & editing. Yuee Zeng：Writing - review & editing.

Declarations

Competing interests
The authors declare no competing interests.

Additional information
Supplementary Information The online version contains supplementary material available at https://doi.org/10.1038/s41598-025-86067-y.

Correspondence and requests for materials should be addressed to Z.C. or Z.C.